Case Studies in Thermal Engineering 28 (2021) 101423

Contents lists available at ScienceDirect

Case Studies in Thermal Engineering

journal homepage: www.elsevier.com/locate/csite

Thermal design of superconducting cryogenic rotor: Solutions to conduction cooling challenges

F. Spaven [a], Y. Liu [a], R. Bucknall [a], T. Coombs [b], M. Baghdadi [a,*]

[a] Mechanical Engineering Department, University College London, UK
[b] Engineering Department, University of Cambridge, UK

ARTICLE INFO

Keywords:
Superconducting motors
HTS tapes
Electrical machines
Cryogenic experiment
Conduction cooling

ABSTRACT

This paper describes the design and testing of the first cryogenic rotor based on conductively cooled superconducting stacked tape pseudo bulks used in a rotating machine with various magnetisation methods. The rotor design demanded a number of unusual features and constraints that required novel, innovative solutions that may be applicable in other designs. The aim of this work is not to create a complete design manual, rather, to suggest some ideas that could be useful to others who are looking to solve similar problems. The outline of the proposed design is followed by a detailed description of the key systems and their interactions. Several innovative design characteristics are discussed, including calculation of liquid cryogenic cooling. Finally, experimental thermal results indicate that the design calculations are reliable and provide reaffirmation of the overall success of the design.

1. Introduction

Since the discovery of High Temperature Superconductors (HTS) in 1986 there has been a great deal of interest in their application to the DC field windings of synchronous electrical machines [1]. The reduction in cooling requirement compared with earlier low temperature superconductors makes such machines an economic prospect with volume, mass and loss reductions of over 50% in large ($>$ 1,000hp) motors and generators as shown in Ref. [2]. These benefits can also offset the increased capital cost due to the superconducting windings, as discussed in Ref. [3].

More recently, investigations have been made into pseudo-permanent magnet machines that rely on magnetised HTS bulks for the rotor field. Such a design can avoid the difficulties associated with the slip rings or contactless current feeds of field windings and the limitations of current permanent magnet technology ([4,5]). As a promising solution, this also raises the issue of magnetising the HTS bulks which is not practical within a conventional motor structure. Hence, alternatives such as field cooling and pulse magnetisation have been explored in Refs. [6,7]. The most challenging proposed method, from a design perspective, is the experimental method of thermally actuated flux pumping where a travelling magnetic wave is created by the radial heating and cooling of a suitable soft magnetic material such as the rare-earth metal Gadolinium. As this Thermally Actuated Material (TAM) passes through its Curie Temperature (around 300 K in this case), its magnetic permeability changes dramatically to produce a series of moving concentric magnetic waves on the surface of the superconductor. As demonstrated in Ref. [8], and unlike conventional methods, this has the

* Corresponding author.
E-mail address: m.baghdadi@ucl.ac.uk (M. Baghdadi).
URL: https://www.ucl.ac.uk (M. Baghdadi).

https://doi.org/10.1016/j.csite.2021.101423
Received 9 May 2021; Received in revised form 24 August 2021; Accepted 2 September 2021
Available online 13 September 2021

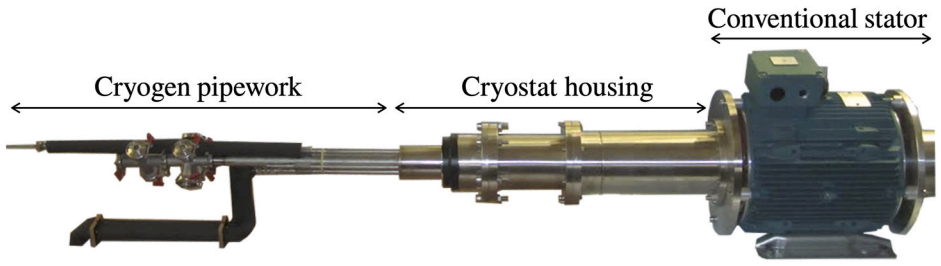

Fig. 1. External view of cryostat and stator. The unusual length allows for long conduction paths and the cryogenic pipework to the left is disconnected before rotation.

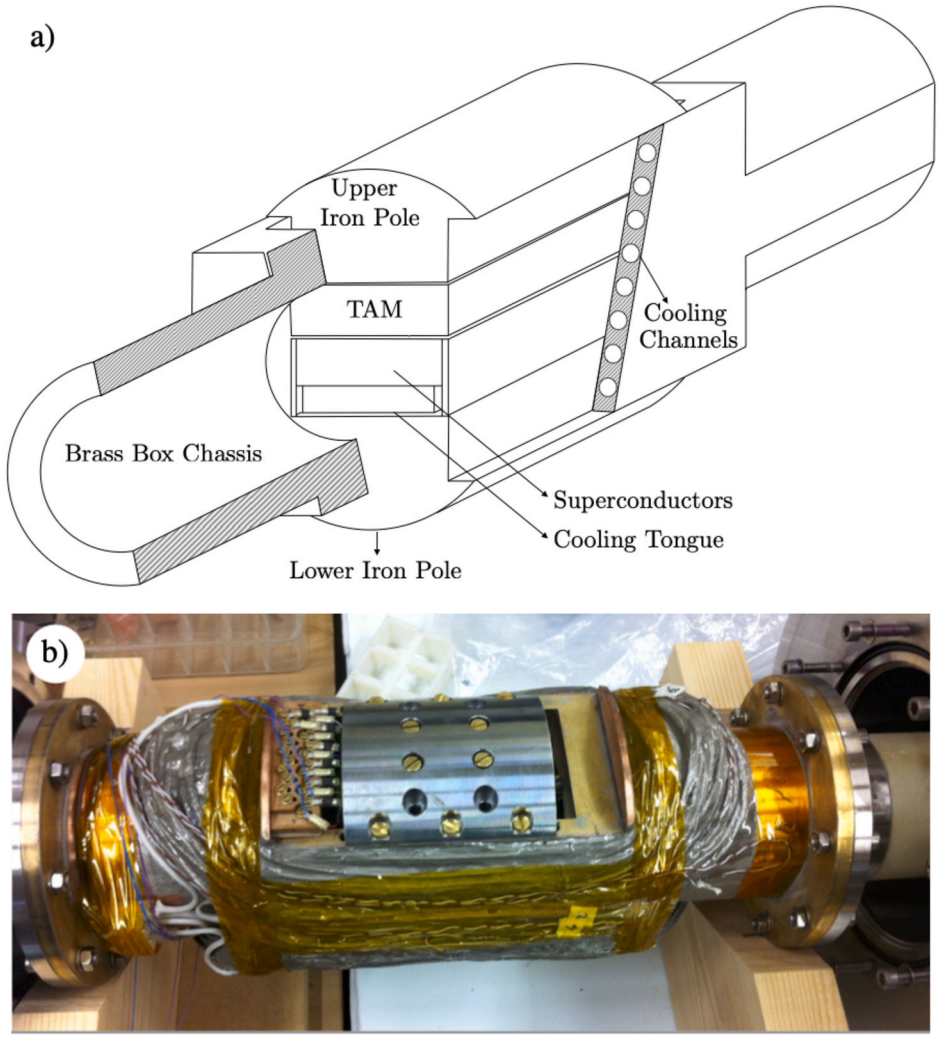

Fig. 2. Rotor assembly a) as isometric cutaway to show general arrangement, outer magnetising coil and cryogenic channels omitted for clarity, and b) photographed ready for insertion into the cryostat showing outer coil (silver) and one custom terminal block.

potential to 'pump' a large magnetic field into a superconducting bulk using a smaller background field, making it a potentially suitable method for rotating machines.

However, further problems arise from cryogenically cooling a rotating component with a variety of solutions presenting themselves. The simplest solution, especially appropriate where both rotor and stator are superconducting, is to immerse the entire machine in a liquid nitrogen bath [9]. This method was successfully demonstrated in the first bulk-type fully HTS motor shown in Ref. [5]; the direct precursor to this stacked tape pseudo-bulk HTS rotor field experiment. Other authors have arrived at more sophisticated systems

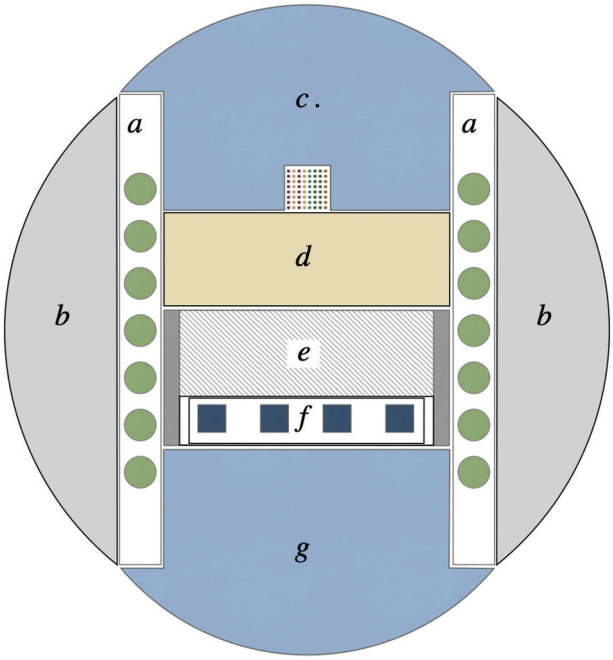

Fig. 3. Representative cross-section showing layout of active components. a. Brass Box, b. Copper Coil, c. Upper Pole Piece, d. TAM, e. Superconducting Cover, f. Nylon Frame, g. Stacked Tapes, h. Helium Tongue, i. Lower Pole Piece. The flux path runs top to bottom (see Fig. 4) through the magnetically active components, (c–i). Cooling is to cryogen channels in the brass box walls and cooling tongue while magnetisation field is supplied by the outer copper winding.

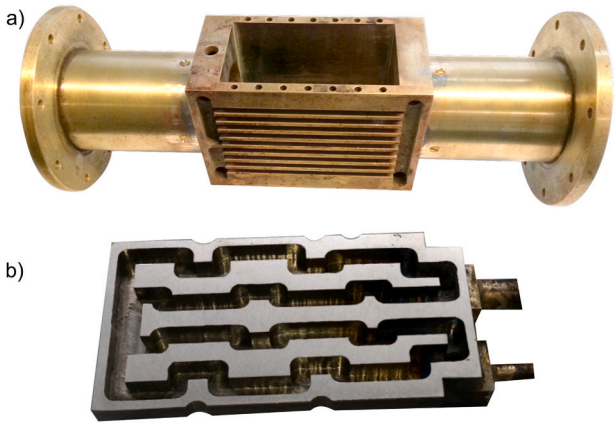

Fig. 4. Cooling channels shown for (a) the Outer Cooling System as cut in the main structural brass box and (b) the Inner Cooling System's soft iron cooling tongue. Convoluted channels refresh the boundary layer, improving critical heat flux.

involving the use of cryogenic seals to supply liquid nitrogen to sealed channels in the rotor assembly and thermally isolating the cold rotor from a conventional warm stator, as might form the basis of a complete solution in a commercial machine [6,10]. Where the stator is also at cryogenic temperatures, it is feasible to cool the rotor by forced convection with helium gas, reducing the quantity of rotating seals required [11,12].

Even setting aside the considerable magnetisation and cooling challenges, the understanding of the behaviour of HTS bulks in rotating machines is still limited and requires further investigation to ascertain their suitability for such an application [2,13].

This paper therefore describes the design and construction of an experimental superconducting rotor that will fit within a commercially available, conventional two-pole stator. The rotor field is to be provided by superconducting bulks or stacked-tape pseudo-bulks in order to investigate their behaviour in rotating machines both under rotating conditions and during the static, magnetising stage. Magnetisation to produce a large field in a conventional motor architecture is non-trivial [6] and a range of possibilities including field-cooling and pulse magnetisation will be investigated. The rotor will also be designed to allow for testing of experimental thermally actuated flux pumping [8]. These requirements, with the associated physical bulk and large cooling

requirements, led to some of the greatest design intricacies but many of the methods and concepts described here will be of more general practical use in experimental cryogenic rotor design.

2. General design elements of the superconducting rotor

The design brief called for a vacuum cryostat inside the warm stator, as illustrated in Fig. 1, containing a rotor mounted on suitable cryogenic bearings. Due to the large thermal loads of the flux pump, TAM heaters and rotor mounted coil, it was decided in this case to use semi-closed loop liquid nitrogen to provide adequate cooling power for chilldown (cooling to cryogenic temperature), magnetisation and static tests. For simplicity it was also decided to forego rotating seals for the liquid cooling circuits and operate the rotor in two distinct modes: 1) static mode, which can be used in chilldown, magnetisation and locked rotor tests; and 2) free rotating mode, which is disconnected from the cooling systems. Note that during the free rotation mode, no active heat loads are present in the stator and good thermal insulation will ensure an adequate experimental run time.

The final rotor design is based around a brass chassis, the centre of which is a hollow box, open top and bottom to permit insertion of magnetic components, with a hollow brass tube protruding from each end to mount to Glass-Fiber Reinforced Plastic (GFRP) shafts. This is shown in Fig. 2(a) as an isometric cutaway and Fig. 2(b) photographed ready for insertion into the cryostat. Fig. 3 shows a diagrammatic cross-section through the working section of the rotor with main components labelled. The salient aspects of the design are discussed in further detail below.

2.1. Modular design

Although the rotor has been designed to meet the expected criteria required to explore the phenomena of flux pumping, other HTS magnetisation methods and the behaviour of stacked-tape superconductors in a rotating machine, the design must also be modular and flexible enough to minimise rework required for extensive future modification as the technologies being tested are developed further. Fig. 3 shows diagrammatically how the various components are assembled into the brass box with the only non-removable part being the helium cooling tongue which, although restrained by its associated pipework, has some allowable vertical movement. This provides a flexible working space through the centre of the brass box, in which various components can be placed as required in future experiments. As well as comprising part of the magnetic circuit, this space also has free access to the high temperature cooling system via the box walls, to the low temperature cooling system via the helium tongue, and wiring via terminal blocks at each end of the machine (as shown in Fig. 2(b)). Such a configuration can maximise the ability to reconfigure the experiment in future. Such a flexibility proved vital when it was later decided to insert a superconducting winding into the Upper Pole Piece to increase the magnetisation field, Section 3.4.

2.2. Electrical design

Due to the large number of data and power systems contained within the rotor, the wiring loom consists of 84 separate wires ranging from slim signal wires up to 2 mm diameter cables for the 10A coil current feed. This enabled a large amount of data to be gathered. Six temperature sensors were provided for both the superconductor and the TAM as well as at several critical locations within the coil. Flux density profile was measured via Hall probes spread throughout airgap between the superconductor and TAM. Finally, six separate heaters were provided for both the superconductors (to modulate critical current) and the TAM (to control the transition across the Curie temperature). Finally, a pair of current carrying cables were provided for both the large copper coil and the smaller HTS coil inserted in the Upper Pole Piece.

This bundle is fitted down the hollow shaft of the rotor, only 60 mm in diameter, alongside four 10 mm diameter cryogen pipes, and linked to the outside world by four vacuum rated connectors.

Wiring within the rotor is more complex. The 18 simplest connections, primarily current feed and temperature sensing for the copper coil, are hard wired to minimise occupied volume while the remaining 66 must be removable for disassembly and modification. Due to the extremely limited available volume, suitable commercial connectors cannot be found and three 22-way screw terminal blocks were especially designed and machined from Tufnol to fit within the arc available at each end of the brass box, as shown in Fig. 2 (b). Such a design leaves space for a fourth similar 22-way terminal block if required in future. The remaining problem is running part of the loom through the space-constrained active part of the rotor. This was achieved by machining a channel through the upper pole piece (Fig. 3) which was sized, by calculation, to statically balance the rotor while leaving the magnetic path unaffected.

2.3. Magnetic design

The magnetic characteristics of the proposed HTS motor were thoroughly discussed in Refs. [14–17]; this section outlines the mechanical and thermal design features required to facilitate these magnetic circuits.

In order to produce a nominally sinusoidal flux distribution in the air gap around the poles the pole ends are shaped and the overall iron cross-section is maximised throughout to minimise the current required during magnetisation of the superconductor. This maximization of permeance in the magnetic circuit is hindered in three major ways. Firstly, the very high temperature gradients within the device (up to 300 K per mm) require vacuum gaps containing super-insulation to prevent conduction and minimise radiation with these vacuum gaps having a relative permeability of unity.

Secondly, the largest gap occurs between the rotor pole pieces and the stator, and it must accommodate the stainless steel cryostat

wall with a small assembly clearance outside and adequate clearance inside to prevent contact under the worst case imbalance and vibration during rotation.

3. Thermal design of superconducting cryogenic rotor

3.1. Outer cooling system

The primary cooling system, which is responsible for extracting most of the heat from the device, acts by conducting heat away from its origin to the walls of the brass box. The heat is extracted by the boiling of liquid nitrogen which flows through machined channels (Fig. 4). Heat removed by such a system mainly originates from three sources:

- **Chilldown**: heat must be extracted from all the components in order to reduce the temperature down to the local working temperature (as low as 77 K). As there are no phase changes in the device (except the coolant itself), chilldown is simply a product of each part's heat capacity and change in temperature;
- **Leakage**: at working temperature heat will migrate from room temperature outside the cryostat in to the cold rotor. Convection is virtually eliminated by pumping the cryostat interior down to a high vacuum and conduction is negligible due to the long heat paths of the cryostat design (Fig. 1) combined with appropriate material selection, such as GFRP for the rotor shafts, where possible [3]. The main source of external heat at these low temperatures is radiation from the cryostat walls, calculated to be between 35W and 135W depending on albedo (and so dependent on variables such as state of polish and superinsulation [18]). This heat flow will slowly bring the rotor back up to room temperature when the coolant flow is cut off to allow rotation and therefore must be minimised.
- **Heat Loads**: are present in the design. As discussed below, the copper coil (and to a lesser extent every current carrying wire) produces heat that must be extracted. In addition to this the TAM contains electrical heating elements, active during flux pumping [17], and uses the upper pole piece as a heat sink, relying on it conducting heat away to the liquid nitrogen for proper operation.

Unwanted heat is extracted from the rotor by a semi-closed loop nitrogen cooling system. The principle is simple: liquid nitrogen is injected into the rotor cooling system through one pipe extracting heat from the channel walls (primarily through latent heat required for boiling) and exits through another pipe as a mixture of liquid and gas. In this manner heat will be extracted down to the boiling point of liquid nitrogen: 77 K. For design purposes, however, this is a difficult system to quantify accurately.

Phase-change heat transfer is characterised by the maximum possible heat transfer from a particular liquid per unit area, i.e. the Critical Heat Flux (CHF). To establish this in our system a lower bound was taken from Ref. [19] to give the empirical equation for liquid nitrogen in a long tube, i.e. $G = 20.q_{CHF}$, where G is the mass flow rate per unit area (kg/m^2.s) and q_{CHF} is the specific critical heat flux (W/m^2). A safe (ie. lower) estimate of 6 l/min flow through the brass box cooling channels is equivalent to a mass flux of 250kg/m^{2}s, which is within the ranges suggested in Ref. [20]. This produces an estimated heat flux of $q_{CHF} = 250/20 = 12.5$ kW/m^2. Multiplied by the channel area available in the brass box walls, this gives a total critical heat flux, or maximum possible cooling power of $P_{CHF} = 648W$. However, as this represents the peak cooling power at this flow rate a much lower representative cooling power must be taken for the real system capability in practical use, in this case 50% [21] was selected to give a working figure of $P_{safe} = 324W$.

3.2. Conductive cooling design

Cooling of the coil is a critical factor of the design. As was also found in Ref. [6], the conventional stator used in this experiment is inadequate to produce ample flux for magnetisation so an additional 6000 ampere turns are required from a rotor mounted copper winding. The heat produced by this conventional, resistive winding must be conducted to the nitrogen channels for extraction from the machine. Most of the coil lies directly adjacent to the large cooling panels to provide a short thermal path to the nitrogen channels but heat flow is hindered by the anisotropy of the coil itself.

The thermal conductivity of a coil (or any stranded composite of different materials) is different in the perpendicular and parallel directions and given by Ref. [22]:

$$k_{para} = (1 - \varphi)k_m + \varphi k_c \tag{1}$$

and

$$k_{perp}^{-1} = \frac{1 - \varphi}{k_m} + \frac{\varphi}{k_c} \tag{2}$$

where k_{para} and k_{perp} are bulk conductivity along and perpendicular to the winding, respectively; k_m and k_c are the thermal conductivity of (epoxy) matrix and (copper) wire, respectively and φ is the cross sectional area fraction of copper in the matrix.

The reasons for this can be easily explained: heat travelling 'across the grain' must repeatedly pass through the low conductivity matrix material between the wires; whereas heat travelling parallel to the windings can follow the path of least thermal resistance along the wires rarely having to 'cross' the matrix. In many conventional windings, the 'matrix' is simply the surrounding air but this will provide virtually zero conductivity in the high vacuum surrounding this coil so a solid matrix must be provided, which can also be used to structurally support the coil. Due to the strong dependence of perpendicular thermal conductivity (above) on the conductivity

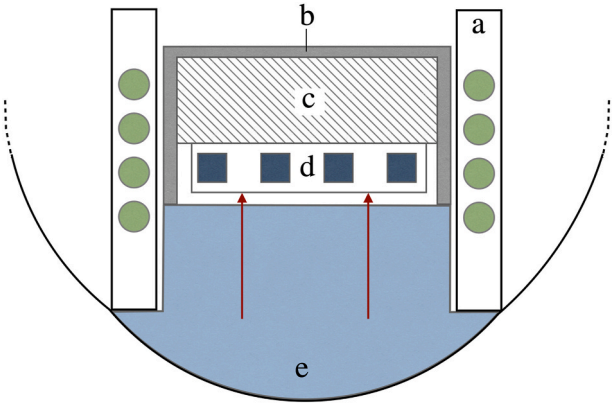

Fig. 5. The Inner Cooling System is kept isolated form the brass box a) by an insulating nylon superconductor frame (b). The Superconductor (c) is chilled by the floating Cooling Tongue (d) by means of insulated jack screws in the Lower Pole Piece (e) exerting force in the direction of the red arrows. Nitrogen cooing channel are shown in green while nitrogen/helium channels are in blue. (For interpretation of the references to colour in this figure legend, the reader is referred to the Web version of this article.)

of the matrix, a high conductivity silver impregnated epoxy was selected into which the coil was manually wound to minimise voids [23].

While this thermal epoxy ensures adequate conduction cooling in the straight sides of the copper coil, the worst cases arise around the end windings (as shown in Fig. 2(b)). Here, a lot of attention was taken to minimise the length of each end turn to reduce copper mass to directly reduce heat production. However, two additional effects are at play.

Firstly, the end windings are furthest from the side panels of the brass box, where the majority of heat extraction occurs. In spite of the better conduction along the wires, the shortest heat path for much of the heat is directly across the winding, in the shorter physical direction, to the ends of the brass box rather than the large cooling panel sides. To aid conduction along this path these parts of the brass rotor chassis have copper plates soldered to the outside as pure copper has a much higher thermal conductivity at cryogenic temperatures than the alloy brass [18].

Heat extraction at the ends of the rotor is provided by cross-bores through the end cheeks of the brass box. At the 'drive' end, this is very well cooled as these cross-bores act as inlet and outlet manifolds for the entire coolant flow but at the 'idle' end, flow must be forced by making the cooling channels in the wall of the brass box asymmetric. Careful examination of Fig. 4 will show five cooling channels connecting to the lower inlet and four connecting to the upper inlet. The opposite side (not visible) is rotationally symmetric, not mirrored as might be expected. This ensures an easier path in for fluid into one side of the box and out from the other, forcing some degree of flow through the 'idle' end cross-bores and cooling to the idle end of the rotor coil.

Secondly, to ensure a constant background field, the coil will be operated at constant current. As resistance increases with increasing temperature [18] and ohmic heating increases with resistance at constant current, there exists the possibility of 'runaway' heating of the device if the rate of heat removal is not adequate. A great deal of care was taken to ascertain the safe operating point (in terms of current, resistance, ohmic losses and temperature) of the coil at critical 'worst case' points, particularly around the end windings. As with many systems, the safe operation of the coil was limited by its weakest point.

3.3. Inner Cooling System

The secondary cooling system is essentially similar to the primary system described above, but with two modes of operation. By cooling with liquid nitrogen, the cooling tongue (Fig. 4) can simply act as a second heat extractor; increasing chilldown rates and ensuring the superconductor is well cooled locally, superconductor critical current and so effectiveness as a magnet being related to temperature [24], as shown in Fig. 5.

The secondary function of the helium tongue is further cooling by liquid helium which boils at 4 K, much lower than nitrogen [18]. This will produce higher critical currents in HTS or allow the use of low temperature superconductors, which do not exhibit superconductivity at 77 K. To this end, the low temperature system is thermally isolated from the high temperature system (which almost completely encloses it) in the same way that the high temperature system is isolated from the outer cryostat wall.

Due to the mechanical link between the low temperature system and its surroundings, conduction is the dominant form of heat transfer: 9.9W at a working temperature of 4 K. Radiative heat transfer is calculated at only 4.4W due to the small surface area and lower temperatures of its surroundings, being almost entirely enveloped by the low temperature system which is already chilled down to 77 K.

Liquid helium cooling is by the same mechanisms as the liquid nitrogen cooling described above although the system is, in fact, sized for the worst case which is cooling with liquid nitrogen while using electrical heaters to modulate superconductivity by temperature; for example to allow experiments with field cooling much more rapid than the bulk chilldown time. 135W is required for this which, by the method described above, can be achieved with a nitrogen flow rate of 2.2 litres per minute.

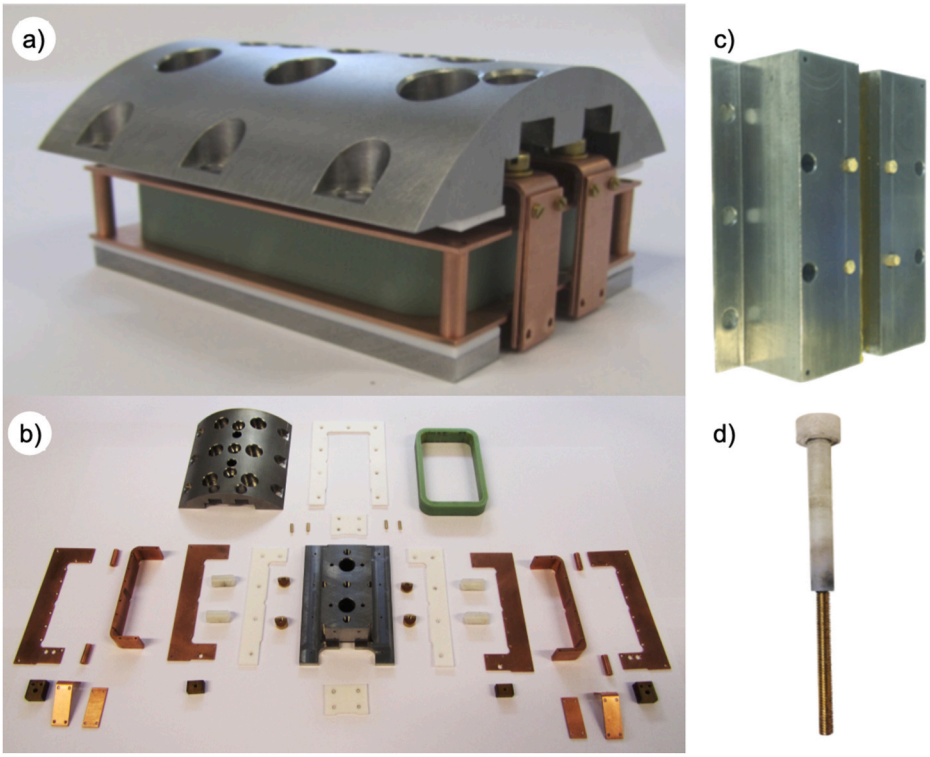

Fig. 6. Modified Pole Piece allows a superconducting tape to be wound on a fibreglass former (green) and chilled via an expandable copper shroud: (a) assembled without superconducting winding and (b) disassembled showing various materials used. (c) Wooden pushrods with low thermal conductivity at cryogenic temperatures exert pressure on the Helium Tongue to increase thermal conductivity. (d) Neutral-contraction stud assembly: brass stud provides strength where diameter is limited while nylon stud holder matches thermal contraction with the surrounding components. (For interpretation of the references to colour in this figure legend, the reader is referred to the Web version of this article.)

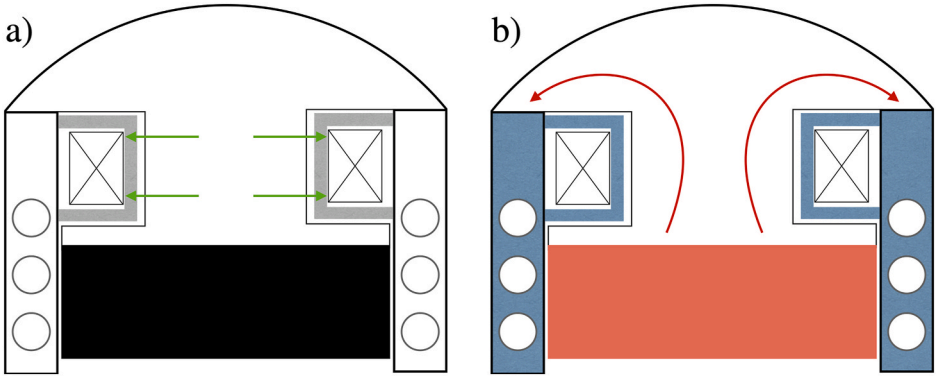

Fig. 7. Diagram of a) clamping action of copper shroud and b) the resulting thermal effects.

It is worth noting that the Helium Tongue cooling channels of Fig. 4(b) are not as simple as the straight lines of the main Brass Box cooling channels of Fig. 4(a). There are two main reasons for this decision. Firstly, as flow proceeds along a straight-sided tube the fluid nearest the wall heats up and, in the case of phase-change cooling, will ultimately boil. In either case the cooling power is reduced but this effect can be minimised by introducing changes of direction such as those shown in Fig. 4(b) to induce turbulent mixing and force cooler fluid against the channel wall. With no direct prior experience of helium cooling, the extra effort in manufacture was considered to be prudent. Secondly, the physical and magnetic loads are not evenly distributed across the Helium Tongue and certain areas, for example where the pushrods operate (see Section 3.5.1), would benefit from a solid section. By convoluting the channels in this way, solid material could be provided where it was most beneficial while simultaneously improving the CHF.

3.4. HTS windings

One of the key design priorities for this rotor was adaptability, allowing for future modifications to change the experimental arrangement with a minimum of work in order to maximise the life of the machine as the technologies under investigation are developed. As a perfect illustration of this, it was decided to supplement the copper winding with a smaller HTS coil, Fig. 6. This addition of a new system into an already tightly packed assembly was not trivial but showed the extremely flexible nature of the modular design employed.

Physical space was found for a rectangular 'racetrack' coil in the upper pole piece, around the six studs that support the TAM. While large enough to contain a coil of sufficient size, the upper pole piece acts as a heat path between the heated TAM and the cooling channels of the brass box walls. As such, the iron surrounding the HTS coil will be roughly halfway between nitrogen temperature (77 K) and the Curie Temperature of the TAM (approximately 300 K) and so well above the HTS critical temperature (95 K); it would not behave as a superconductor if simply bolted to the pole piece. As shown in Fig. 7(a), the solution found was to insulate the HTS coil from the surrounding warm iron and provide a good thermal connection to the adjacent brass box walls and the outer cooling system.

This was achieved through an intricate but satisfying method whereby the superconducting coil, wound on a stiff GFRP former is loosely encased in a two-part copper shroud which is itself thermally isolated from the new pole piece by nylon 'runners' on which it is free to slide. This new pole piece supports the TAM in the original way and slots into the top of the brass box just as before. Once screwed into position, a pair of fully floating (and therefore thermally separate) wedges are tightened by means of screws accessible from above, forcing the copper shroud apart and clamping it to the interior of the brass box, as depicted in Fig. 7(b).

The correct design and choice of materials is essential. The high thermal conductivity copper shroud, combined with a high clamping force, efficiently conducts heat away to the outer cooling system's nitrogen channels. Simultaneously, the very low thermal conductivity nylon runners, very low contact pressures of the fully floating arrangement and the ubiquitous vacuum environment minimise thermal conduction into the superconducting coil from the warm iron pole piece, itself heated by the TAM. Thus, two mechanically intertwined components can be assembled together but kept thermally separate in use.

3.5. Material selection

3.5.1. Wooden pushrods

In order to ensure a good thermal connection to the Superconductor, a method was required to force the Helium Tongue away from the Lower Pole Piece without thermally linking the two components or damaging the helium tongue. A solution was found whereby a jack screw inside the Lower Pole Piece exerts pressure on a low thermal conductivity pushrod which, in turn, presses on the cooling tongue, Fig. 6(c). To work successfully, the pushrod material must exhibit low thermal conductivity at cryogenic temperatures as well as low thermal contraction. Oriented strand GFRP would be suitable but a more convenient solution was found in ordinary hardwood dowel which shows a low thermal contraction along the grain and has found use in other cryogenic applications [25,26].

3.5.2. Neutral contraction studs

Experience gained in previous cryogenic experiments highlighted an issue arising from the clamped structure of the superconductor, cover plate and nylon frame. During chilldown, the nylon frame will contract substantially more than the metal studs, clamping pressure will reduce and components may be able to shift out of position; reducing experiment reliability. A conventional solution is to use studs of a similar material to the surrounding structure but in this case there is insufficient space for a stud made of nylon, due to the larger diameter required by the weaker material. The problem was solved by fabricating nylon stud holders that were inserted through the pole piece, where space *is* available, for the smaller diameter metal studs to screw into, as shown in Fig. 6 (d). In this case, the brass stud provides strength where diameter is limited while nylon stud holder matches thermal contraction of HTS stacked-tape holder. By suitably sizing the proportions of nylon and metal stud, differential contraction can be effectively eliminated.

4. Experimental results and discussions

4.1. Chilldown process

Chilldown is the process whereby the rotor is initially brought down to cryogenic temperatures before experiments in the steady state can begin. Nitrogen phase-change cooling is complicated even further during chilldown by the very high temperature difference between the boiling Nitrogen and the cooling channel walls, initially around 223 K. Under these conditions cooling rates are substantially reduced as gaseous nitrogen produced at the channel walls forms a low thermal conductivity 'cushion' preventing liquid nitrogen from coming into contact with the wall. This effect is similar to a drop of water skittering over a kitchen hotplate without boiling away. Again this is an incredibly complex problem which changes dramatically in time as the system temperatures alter [21].

To establish an order of magnitude figure for chilldown rate, a comparison between average heat flux during a chilldown procedure vs. CHF was taken from Ref. [21], showing average heat flux to be approximately 40% of CHF. This gives our system a time average chilldown heat flux of approximately 684W $\times$ 40% = 274W. Subtracting the incoming radiation of 36W–135W gives a sum average heat removal of 139W–238W at steady state.

Incoming radiation varies with temperature but by assuming it is constant a rough-and-ready upper bound to the chilldown time can be found from:

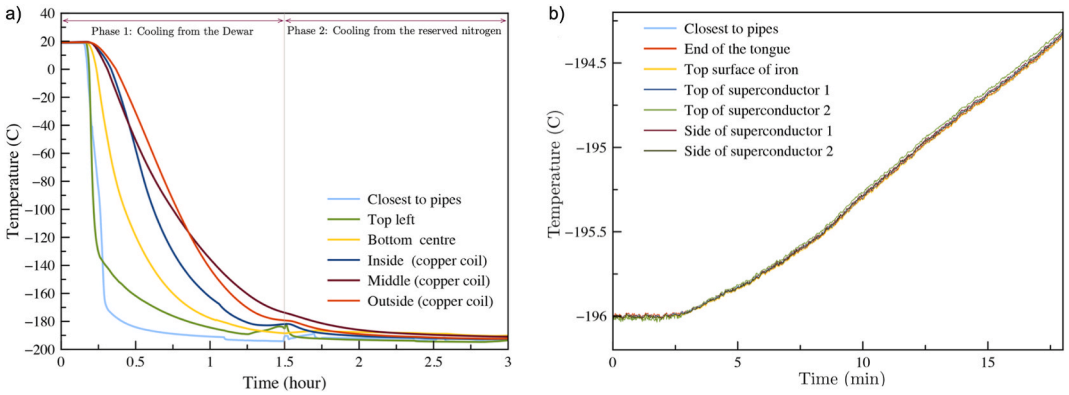

Fig. 8. a) Rotor Chilldown process with liquid nitrogen. Total cooling time to a bulk temperature of 77 K is 2.5 h. b) Warm up process of HTS superconducting rotor. The low rate of cooling resulted in a window of approximately 165 min of superconductivity for rotation tests.

$$t = \frac{C_{tot} \times \Delta T}{P} \tag{3}$$

where t is chilldown time, C_{tot} is total heat capacity (an approximation as this will vary with temperature, but far from the vaguest approximation made here), ΔT is the change in temperature and P is the cooling power.

This gives a range of upper bounds between $\frac{6.1kJ/K \times 223K}{235J/s} = 5,788s$ and $\frac{6.1kJ/Kx223K}{36J/s} = 37,786s$ that is between 1.5 h and 10.5 h. While only indicative, this clearly emphasises the need to minimise incoming radiation and the wide range (due to real world unknowns) suggests more accurate calculation would not be worthwhile.

Figure 8 demonstrates the chilldown run while operating the outer coolant circuit only. This process was carried out in two stages. Initially nitrogen flows from a pressurised Dewar, through the rotor and into a collector tank where the nitrogen gas is allowed to escape. After 1.5 h, the Dewar has emptied and flow is taken from the collector tank under a hydrostatic head of approximately 1.5 m, the resulting interruption in continuous cooling is visible in Fig. 8(a). The total time for cooling to a bulk temperature of 77 K is about 2.5 h, well within the range predicted by the upper bound calculation above, after taking reasonable measures to minimise radiation effects.

4.2. Warm up process

The most tenuous stage of operation is when the coolant flow is stopped so that the machine can be rotated. In this case there is no active heat load, as the wiring is disconnected, which allows both conduction and convection to be neglected. The rotor is heated by radiation from the warm outer wall of the cryostat. Consequently, the window for testing is quite limited before the superconductors return to their normal state and lose their magnetisation. In this design, an 18 K temperature rise will cause this to occur. Also, based on the estimated thermal capacity at this temperature (6.1 kJ/K) and the heating rates above, the rotor should remain in a superconducting state for between 13 min and 45 min. This demonstrates the importance of high albedo and good superinsulation in practice and quick release fasteners for wiring and coolant circuits to minimise delay before tests can begin.

Fig. 8(b) shows the temperature curves following disconnection from the coolant. It should be noted that very little loss occurs after flow is stopped until minute 3 when the piping is disconnected. This illustrates two points: firstly it is difficult and time consuming to uncouple pipework covered in ice and secondly there is a major source of heat flow through the pipes once air is admitted.

The full decoupling of the frosted wiring and plumbing connectors took around 15 min before rotation could take place. Nevertheless, an extremely low rate of cooling of 0.1 K per minute, after pipes were disconnected, allowed a window of approximately 165 min of superconductivity for rotation tests, which was much longer than expected.

5. Conclusion

A design for an experimental cryogenic, superconducting synchronous rotor has been outlined along with the cryogenic cooling calculations used to size some of the components. Due to large real-world unknowns simple calculations based on safe, rather than precise, figures were used to ensure the success of a complex project. Examples of specific problems encountered during the design have been discussed and solutions, often innovative and previously unknown to the authors, have been suggested. The rotor has been constructed and results are presented that confirm the reliability and accuracy of the cooling calculations.

Author statement

Fred Spaven: Design, Modeling, Experimental, Writing, Reviewing, Editing. Yuanchang Liu: Analysis, Writing, Richard Bucknall: Analysis, Writing, Timothy Coombs: Supervision, Mehdi Baghdadi: Design, Modeling, Experimental, Analysis, Visualization, Writing,

Reviewing, Editing, Supervision.

Declaration of competing interest

The authors declare that they have no known competing financial interests or personal relationships that could have appeared to influence the work reported in this paper.

References

[1] D. Driscoll, A review of superconducting motor technology development, IEEE Power Engineering Society Winter Meeting. Conference Proceedings (Cat. No. 01CH37194 2, IEEE, 2001, pp. 438–441, 2001.
[2] V. Climente-Alarcon, N. Mineev, A. Smara, L. Tomkow, B.A. Glowacki, Superconducting magnetic heterostructured components for electric motor applications, IEEE Trans. Appl. Supercond. 30 (4) (2020) 1–5.
[3] R. Schiferl, A. Flory, W.C. Livoti, S.D. Umans, High temperature superconducting synchronous motors: economic issues for industrial applications, in: Record of Conference Papers-IEEE Industry Applications Society 53rd Annual Petroleum and Chemical Industry Conference, IEEE, 2006, 2006, pp. 1–9.
[4] E. Kurbatova, P. Kurbatov, P. Dergachev, O. Molokanov, Electromagnetic analysis of hts generator with bulk superconductor, in: 2018 20th International Symposium on Electrical Apparatus and Technologies (SIELA), IEEE, 2018, pp. 1–4.
[5] Z. Huang, W. Xian, M. Zhang, M. Chudy, Y. Chen, Z. Zhong, M. Baghdadi, W. Wang, F. Spaven, K. Matsuda, et al., Control and operation of a high temperature superconducting synchronous motor, IEEE Trans. Appl. Supercond. 23 (3) (2012), 5200204–5200204.
[6] X. Feng, G. Gao, K. Davey, M. Werst, R. Hebner, R. Weinstein, D. Parks, R. Sawh, Radial flux high temperature superconductor motor using bulk trapped field magnets ieee int. electric machines & drives conf.(miami, fl, may 2009) pp. 458–64 oswald b, krone m, soll m, strasser t, oswald j, best kj, gawalek w and kovalev l 1999 superconducting reluctance motors with ybco bulk material ieee trans, Appl. Supercond (9) (2009) 1201–1204.
[7] K. Tsuzuki, Y. Suzuki, S. Yamamura, S. Kadowaki, D. Oikawa, H. Andoh, T. Tsukamoto, Design of bulk hts rotating machine using closed-circuit magnetization, IEEE Trans. Appl. Supercond. 29 (5) (2019) 1–5.
[8] Y. Yan, C. Hsu, Z. Hong, W. Xian, W. Yuan, T. Coombs, A novel design of thermally actuated magnetization flux pump for high temperature superconducting bulks, IEEE Trans. Appl. Supercond. 21 (3) (2010) 1568–1571.
[9] V. Climente-Alarcon, A. Smara, L. Tomkow, B.A. Glowacki, T. Reis, Testing of surface mounted superconducting stacks as trapped-flux magnets in a synchronous machine, IEEE Trans. Appl. Supercond. 30 (5) (2020) 1–8.
[10] A. Perez, R. Van Der Woude, R. Dekker, Rotor cooling concept for the assumed superconductive motor, in: IOP Conference Series: Materials Science and Engineering, vol. 502, IOP Publishing, 2019, 012139.
[11] L. Tomkow, N. Mineev, A. Smara, V. Climente-Alarcon, B.A. Glowacki, Heat extraction from hts tape stacks applied in a superconducting motor in different cooling conditions, in: Journal of Physics: Conference Series, vol. 1559, IOP Publishing, 2020, 012088.
[12] L. Tomkow, I. Harca, K. Machaj, A. Smara, T. Reis, B. Glowacki, Experimental system for testing a superconducting motor at temperatures close to 15 k, Cryogenics 112 (2020) 103206.
[13] C.D. Manolopoulos, M.F. Iacchetti, A.C. Smith, P.M. Tuohy, X. Pei, M. Husband, P. Miller, Design of superconducting ac propulsion motors for hybrid electric aerospace, in: AIAA/IEEE Electric Aircraft Technologies Symposium (EATS), IEEE, 2018, 2018, pp. 1–9.
[14] M. Baghdadi, H.S. Ruiz, T. Coombs, Crossed-magnetic-field experiments on stacked second generation superconducting tapes: reduction of the demagnetization effects, Appl. Phys. Lett. 104 (23) (2014) 232602.
[15] M. Baghdadi, H.S. Ruiz, T.A. Coombs, Nature of the low magnetization decay on stacks of second generation superconducting tapes under crossed and rotating magnetic field experiments, Sci. Rep. 8 (1) (2018) 1–9.
[16] A. Campbell, M. Baghdadi, A. Patel, D. Zhou, K. Huang, Y. Shi, T. Coombs, Demagnetisation by crossed fields in superconductors, Supercond. Sci. Technol. 30 (3) (2017), 034005.
[17] J. Geng, K. Matsuda, L. Fu, J.-F. Fagnard, H. Zhang, X. Zhang, B. Shen, Q. Dong, M. Baghdadi, T. Coombs, Origin of dc voltage in type ii superconducting flux pumps: field, field rate of change, and current density dependence of resistivity, J. Phys. Appl. Phys. 49 (11) (2016) 11LT01.
[18] J. Ekin, Experimental Techniques for Low-Temperature Measurements: Cryostat Design, Material Properties and Superconductor Critical-Current Testing, Oxford university press, 2006.
[19] T. Ami, N. Nakamura, T. Tsuruno, T. Higuchi, H. Umekawa, M. Ozawa, Boiling heat transfer and flow characteristics of liquid nitrogen in helically coiled tube, Jpn. J. Multiphas. Flow 24 (5) (2010) 567–576.
[20] S.G. Kandlikar, Handbook of Phase Change: Boiling and Condensation, Routledge, 2019.
[21] K. Yuan, Y. Ji, J. Chung, Cryogenic chilldown process under low flow rates, Int. J. Heat Mass Tran. 50 (19–20) (2007) 4011–4022.
[22] R. Progelhof, J. Throne, R. Ruetsch, Methods for predicting the thermal conductivity of composite systems: a review, Polym. Eng. Sci. 16 (9) (1976) 615–625.
[23] M. Baghdadi, Design and Fabrication of the hts Synchronous Motor Using 2g-hts Stacked tapes, Ph.D. thesis, University of Cambridge, 2016.
[24] A. Koblischka-Veneva, M.R. Koblischka, K. Berger, Q. Nouailhetas, B. Douine, M. Muralidhar, M. Murakami, Comparison of temperature and field dependencies of the critical current densities of bulk ybco, mgb_2, and iron-based superconductors, IEEE Trans. Appl. Supercond. 29 (5) (2019) 1–5.
[25] K.K. Mahato, K. Dutta, B.C. Ray, Emerging advancement of fiber-reinforced polymer composites in structural applications, New Mater. Civ. Eng. (2020) 221–271.
[26] A. Hofmann, The thermal conductivity of cryogenic insulation materials and its temperature dependence, Cryogenics 46 (11) (2006) 815–824.